Supplemental data

Supplemental Figure 1. Expression of genes in the Slit-Robo-Myo9b signaling pathway in lung cancer cells. (A) RT-PCR was performed with specific primers to assess the mRNA levels of corresponding genes in primary lung cancer samples (lower part: 3 pairs of lung tumor samples together with their adjacent non-tumor control tissue samples) or lung cancer cell lines (upper part) (H1299, A549, H719 and H841) and HEK293 cells. Lane 6 contains the negative control reaction (H1299) in which the reverse transcriptase was omitted. **(B)** Detection of Robo1 and Myo9b proteins in different lung cancer cell lines by Western blotting using corresponding specific antibodies. Actin was used as a loading control. **(C)** Wound-healing experiments were carried out using A549 cells treated by control, Slit and RoboN preparations. At 0 hr and 13 hr after wound formation, phase-contrast images were taken under an inverted microscope (Scale bar: 100um). Data represent 5 independent experiments. **(D)** Quantification of the cell migration distance 13 hr after the wound formation. The forward cell migration distance was presented as the mean ± SEM (3 independent experiments; ***: p<0.0001 by Mann–Whitney test). **(E)** GST pull-down experiments were carried out using cell lysates from stable H1299 cell lines overexpressing Slit2 (two groups) or control H1299 cells (Ctr) with GST-RBD/GST-PBD proteins. The active levels of RhoA, Cdc42 or Rac1 were examined by Western blotting using the corresponding antibodies. The actin was shown as an internal control. **(F)** Migration of H1299 cells transfected with myc-tagged CA-RhoA or control plasmids were examined by wound healing assay. The images were taken at 0 hr. and 12 hr (Scale bar: 100um). Data represent 5 independent experiments. **(G)** Quantitative analysis was shown in a bar graph, representing the mean ± SEM for triplicate measurements and *p* value was determined by Mann–Whitney test.

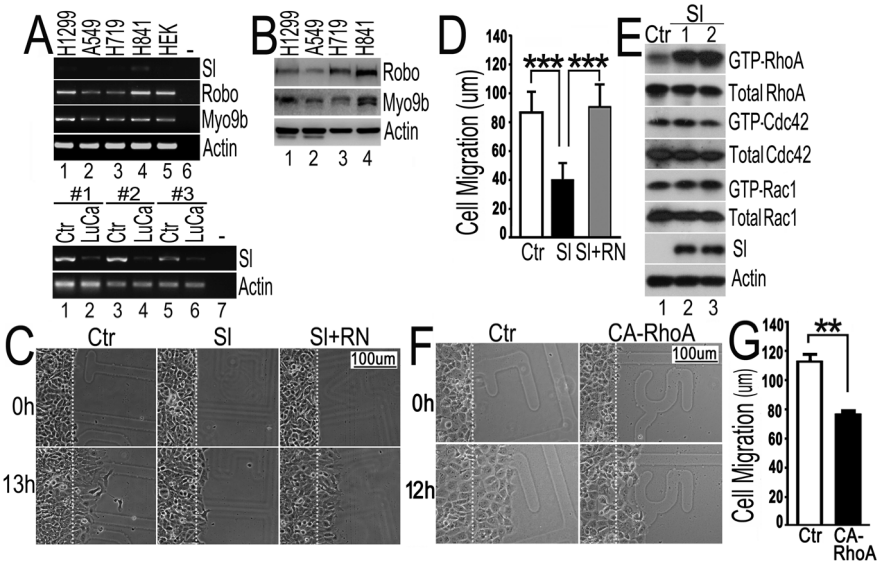

Supplemental Figure 2. Myo9b interacts with Robo1 and mediates Slit2-induced cell migration inhibition and RhoA activation. (A) Interaction of Robo1 with Myo9b was examined in HEK293 cells. Cells transfected with HA-Robo1 or control vector were lysed for immunoprecipitation (IP) using anti-HA antibody following immunoblotting with Myo9b antibody. **(B)** A diagram depicting the full-length (FL) Robo1 and its various deletion mutants. **(C)** Mapping Myo9b interaction domain in Robo1. Immunoprecipitation with anti-HA antibody from H1299 cell lysates transfected with various combinations of plasmids containing Myo9b and Robo deletion mutants, followed by immunoblotting with anti-Flag antibody. The Robo1 mutant lacking the intracellular domain (△ICD) was served as the negative control. **(D)** A diagram illustrating the wild-type Myo9b and different Myo9b mutants. **(E)** Co-immunoprecipitation assay was performed to determine the requirement for Myo9b RhoGAP domain in association of Myo9b with Robo1. Antibodies used in immunoprecipitation and immunoblotting were as indicated. **(F)** The purified MBP-His_6- Robo-ICD and MBP (maltose binding protein) proteins were shown in lanes 3 and 2 respectively with protein size markers in lane 1. **(G)** Yeast two-hybrid assay with Robo-ICD and Myo9b C1-GAP or GAP domain. **(H)** H1299ctr and H1299Slit (stably expressing Slit) cells transfected with siRNA against Myo9b (siMyo9b-2) or control siRNA (siCtr) were examined for cell migration using the wound-healing assay. Representative images were shown at 0 hr and 12 hr after wound formation (Scale bar: 100um). Data represent 5 independent experiments. **(I)** The distance of cell migration in different treatment groups was quantified as the mean ± SEM (***: p<0.0001; Mann–Whitney test). **(J)** H1299Slit cells were transfected with siMyo9b-2 or siCtr and GST pull-down assay and immunoblotting were performed to measure the RhoA activity.

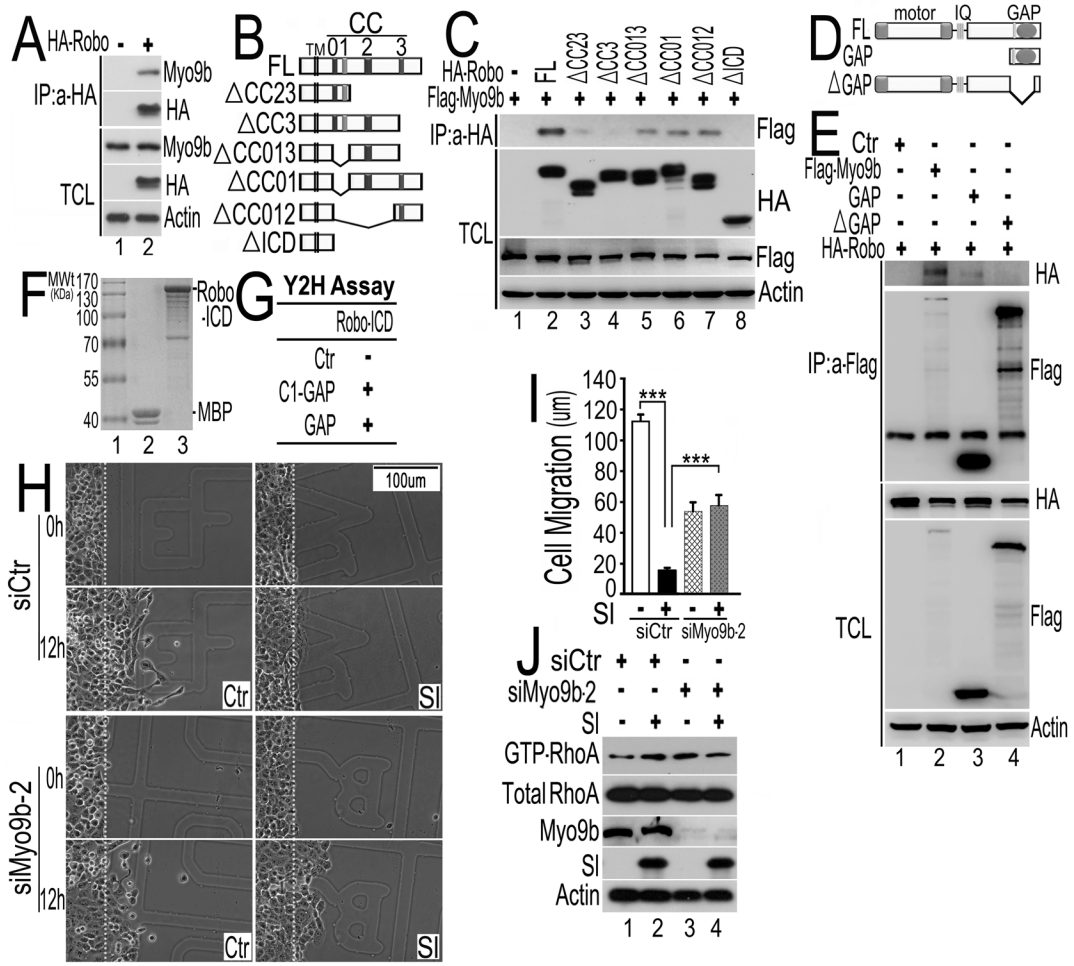

Supplemental Figure 3. No significant difference was observed in cell proliferation between control and siMyo9bs-mediated H1299 cells treated with Slit (Sl) conditioned media. (A) H1299 cells transfected with siRNA control or siMyo9b were treated with the control or Sl conditioned media, followed by fixation in methanol and staining with crystal violet (0.1%). Representative images of stained cells in different groups are shown (Scale bar: 200um). Data represent 5 independent experiments. **(B)** The cell numbers in corresponding groups were quantified using ImageJ software. Data were represented as the mean ± SEM in 3 independent experiments and analyzed by one-way ANOVA.

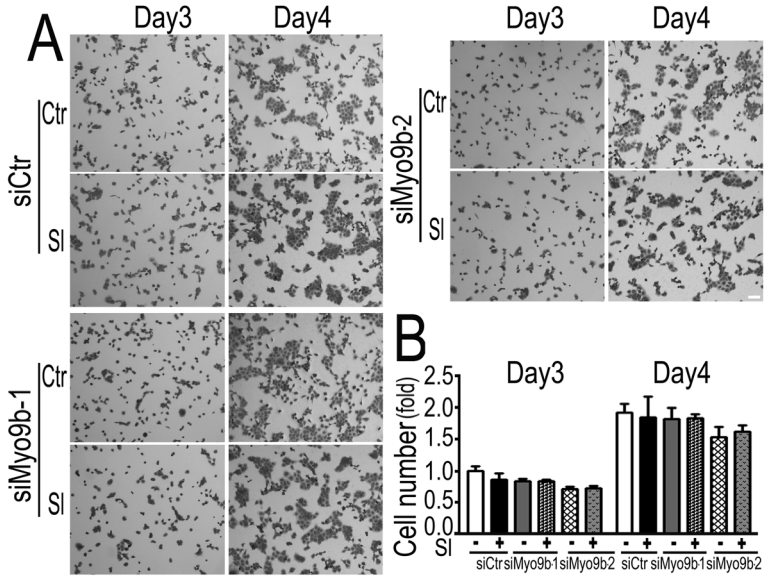

Supplemental Figure 4. Myo9b inhibits RhoA activity. (A) H1299 cells were transfected with siCtr or siMyo9b-1/2 and the active levels of RhoA, Cdc42 or Rac1, were detected by Western blotting in cell lysates following the GST pull-down experiment (GST-RBD for GTP-RhoA, GST-PBD for GTP-bound Cdc42 or Rac1). The total input protein levels were shown in corresponding panels. Efficient downregulation of Myo9b expression by its specific siRNAs was shown by Western blotting using anti-myo9b antibody. Actin was used as an internal control. **(B)** H1299 cells were transfected with the control vector (Ctr), or plasmids encoding either the full-length Myo9b (FL), Myo9b lacking the RhoGAP domain (△GAP), the C1 motif and RhoGAP domain (C1-GAP) or the RhoGAP domain of Myo9b (GAP). Cell extracts were subjected to GST pull-down assays. **(C)** HEK293 cell lysates were prepared following transfection using myc-RhoA, Myc-Cdc42 or Myc-Rac1 plasmids. Cell lysates were incubated with purified GAP protein at different concentrations (1ug, 5ug, 10ug, 25ug and 50ug) at 30°C for 10min. GST pull-down experiments were carried out to examine the active levels of corresponding small GTPases. BSA was used as a negative control.

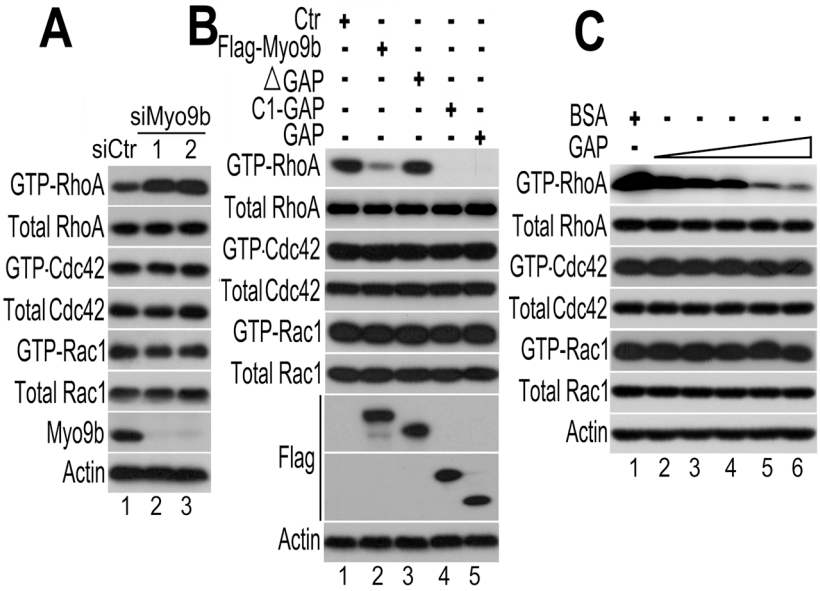

Supplemental Figure 5. Sequence and structural comparison of Myo9b RhoGAP domain with RhoGAP domains in other proteins. (A) Structure-based sequence alignment of the RhoGAP domains from Myo9b (NM_004145.3), GRAF (NM_205194.2), p115 (NM_001666.4), p50rhoGAP (NM_004308.3), ArhGAP15 (NM_018460.3) and cdGAP (NM_020754.3). The identical residues and highly conserved residues are colored in red and green, respectively. The residue numbers of Myo9b RhoGAP domain and the secondary structures are marked on the top. The residues responsible for the formation of Patch II are highly variable and highlighted by a magenta box and the region connecting αA1 and αB is variable and indicated by a black box. **(B)** Structural comparison of Myo9b and p50rhoGAP RhoGAP domains. A ribbon diagram of the superimposed RhoGAP domain structures of Myo9b and p50rhoGAP. The Myo9b and p50rhoGAP RhoGAP domains are colored in green and red, respectively. The secondary structures and the N- and C-termini of the domains are marked. **(C-E)**, A detailed comparison of the structure of Myo9b and p50rhoGAP RhoGAP domains. The central core four-helix bundles of two domains can be well superimposed, as shown in panel C. In contrast, the neighboring αA1 and the loop between αA1 and Ab show some differences between the two structures, as depicted in panel D. Moreover, the last helix αG of Myo9b is much longer than that of p50rhoGAP, although the functional significance of this feature is unclear at the current stage as shown in panel E.

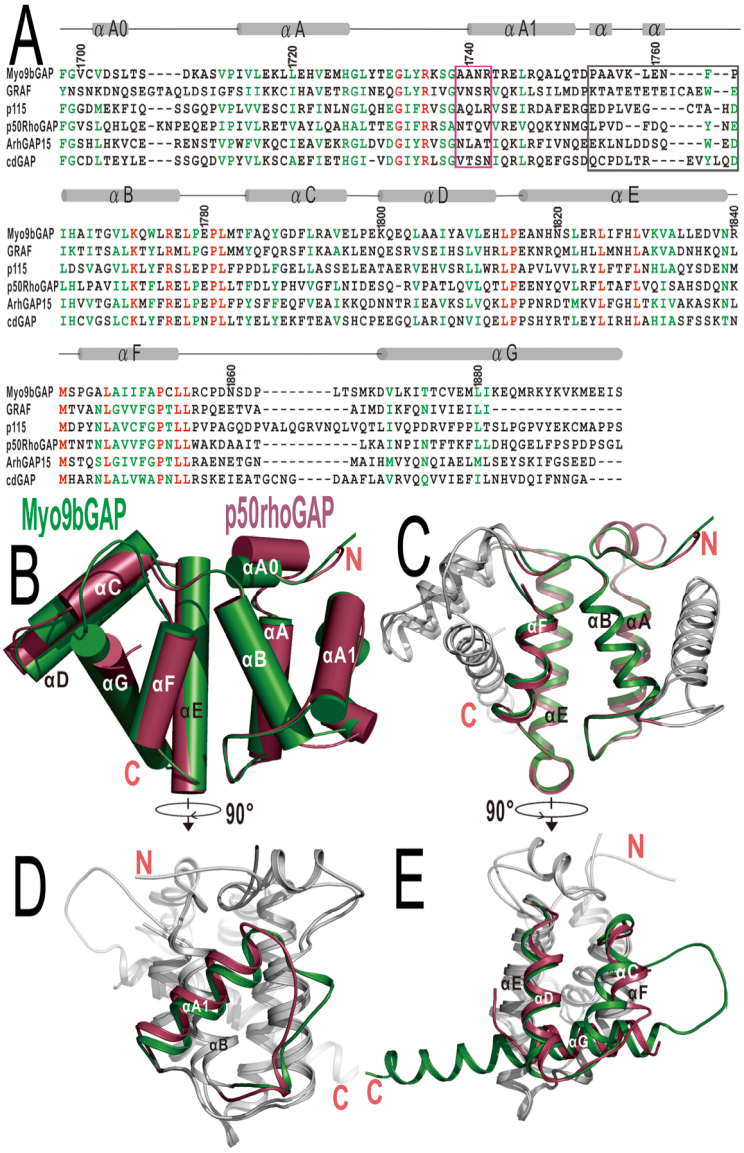

Supplemental Figure 6. The structure of the p50RhoGAP RhoGAP/RhoA complex. (A) A ribbon diagram of the structure of the p50RhoGAP RhoGAP/RhoA complex (PDB code: 1OW3). p50RhoGAP RhoGAP domain and RhoA are colored in light green and dark red, respectively. The GDP and MgF3 are shown as sticks and spheres, respectively. In this complex structure, the Switch I, Switch II and A3 helix of RhoA binds to the concave side of the RhoGAP domain formed by αA1, αB, αF, αG, and the αA/αA1 and αF/αG loops. More interestingly, this binding site of the RhoGAP domain can be further divided into three patches (Patch I, II and III). The active arginine-finger is located in the αA/αA1 loop. **(B)** An "open-book" view of the interaction interfaces between p50RhoGAP RhoGAP domain and RhoA. In this surface drawing, the hydrophobic, positively charged, negatively charged residues and remaining residues are colored in yellow, blue, red and white, respectively. The diagram depicts the direct interaction between the Patch I, II and III in p50RhoGAP domain with the Switch II, Switch I and the A3 helix of RhoA, respectively.

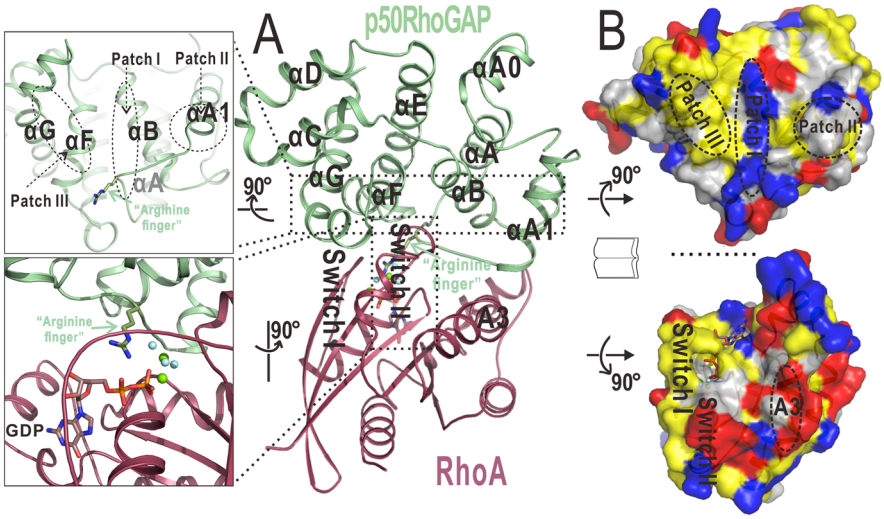

Supplemental Figure 7. Comparison of RhoA, Cdc42 and Rac1. (A) Structure-based sequence alignment of the human RhoA (NM_001664.2), Cdc42 (NM_001791.3) and Rac1 (NM_006908.4) proteins. The identical residues and highly conserved residues are colored in red and green, respectively. The residue numbers of RhoA and the secondary structures are marked above the peptide sequences. The Switch I, Switch II and P-Loop are also marked. The residues in RhoA, Cdc42 and Rac1 responsible for binding to Patch II of the RhoGAP domain are variable and highlighted by orange boxes. **(B** and **C)**, A combined ribbon and stick model illustrates the potential interaction interfaces between Patch II of Myo9b RhoGAP domain and the A3 helix of Cdc42 (B) or Rac1 (C). In this structural comparison, RhoA in the Myo9b RhoGAP/RhoA complex was replaced by Cdc42 (PDB code: 1GRN) or Rac1 (PDB code: 1HE1) to show the potential contacts between Patch II and the A3 helix. In comparison to RhoA, D90 is replaced by S88 in Cdc42; and D90 and E97 are substituted with A88 and A95 respectively in Rac1. It is obvious that the A3 helix of Cdc42 or Rac1 would not be well recognized by the positively charged Path II of Myo9b RhoGAP domain.

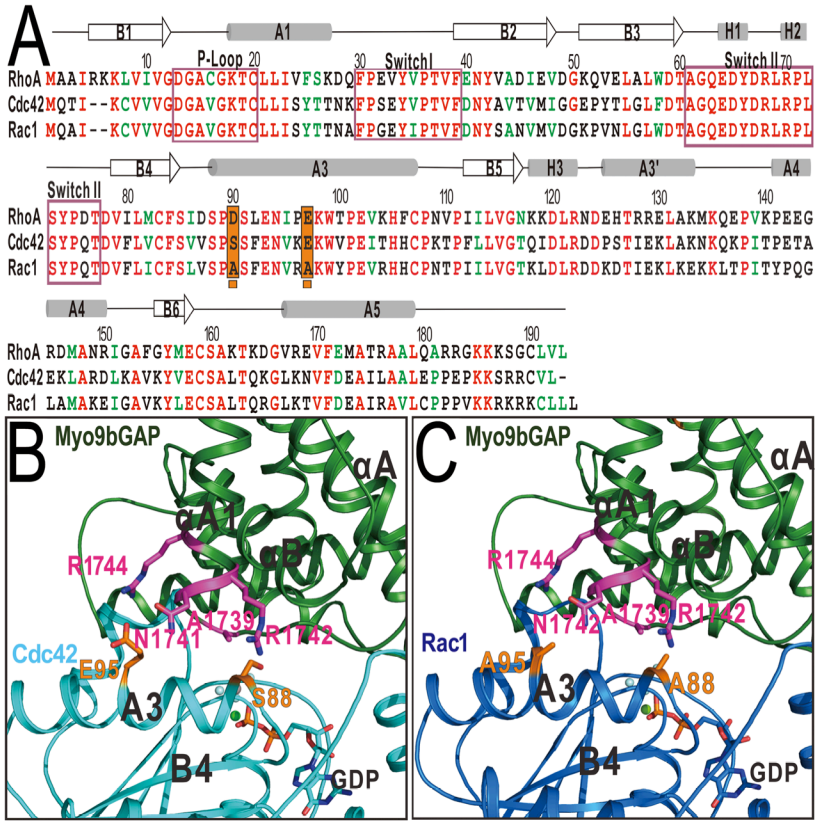

Supplemental Figure 8. Myo9b RhoGAP was capable of inactivating the mutant forms of Cdc42 or Rac1. (A) Myo9b RhoGAP decreased the active level of the Cdc42(S88D/K94P) double mutant, in which serine and lysine at amino acid residue positions 88 and 94 respectively were changed to aspartic acid and proline. H1299 cells were transfected with the RhoGAP domain of Myo9b and plasmids encoding either the wild-type Cdc42 or the Cdc42(S88D/K94P) double mutant. Cell extracts were subjected to GST pull-down assays and Western blotting to measure the activity of Cdc42. **(B)** Myo9b RhoGAP inactivated the mutant form of Rac1. The alanine and arginine at 88, 94 and 95 amino acids of Rac1 were mutated to the corresponding amino acids of RhoA indicated to the Rac1(A88D/R94P/A95E) triple mutant. Extracts from H1299 cells transfected with the RhoGAP domain of Myo9b and plasmids encoding either the wildtype Rac1 or the Rac1(A88D/R94P/A95E) triple mutant were subjected to GST pull-down assays to examine the activity of Rac1. **(C)** Mutations of amino acid residues in helix A3 of Cdc42 increased the binding between Myo9b RhoGAP domain and Cdc42. GST pull-down experiments were carried out examine the interaction of recombinant GST-Myo9b RhoGAP domain and wild-type or mutant forms of myc-Cdc42 from the HEK293 cells. **(D)** Rac1 mutant increased the binding between Myo9b RhoGAP domain and Rac1. The interaction of GST-Myo9b RhoGAP domain with either the wild-type or the triple mutant forms of Rac1 from the HEK293 cells was measured using GST pull-down assay.

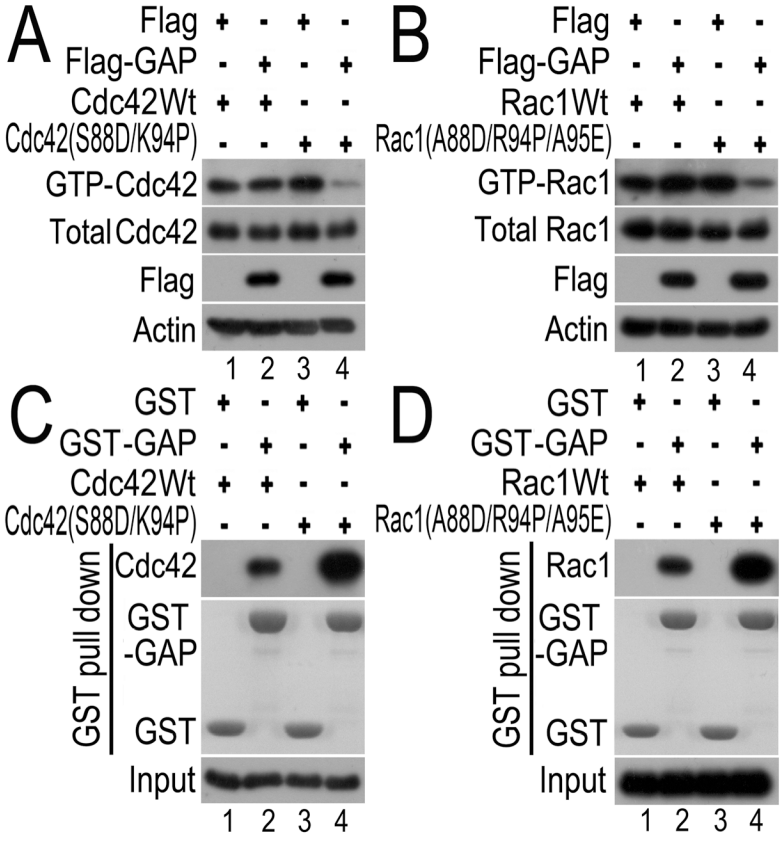

Supplemental Figure 9. Slit2 is down-regulated in lung cancer tissues, with the higher Slit2 expression associated with the longer survival of patients. (A) Slit2 gene expression in patients from Oncomine datasets. The maximum, 75th percentile, median, 25th percentile, minimum of corresponding datasets are indicated in the boxplots. Error bar: 10th-90th percentile. Y-axis: the Slit mRNA level is expressed as Log2 median-centered intensity. P-values were determined by Student's t test (Okayama: n=20/226; Selamat: n=58/58; Landi: n=49/58 for Ctr/LuCa respectively). **(B** and **D)**, Kaplan-Meier plots of overall survival (OS) or progression-free survival (PFS) of lung cancer patients stratified by median levels of Slit2 expression in the CaArray and GSE31210 datasets with Log-rank test p-values displayed. **(C)** Kaplan-Meier plots of OS of lung cancer patients at tumor grade III or with lymph node metastasis stratified by median Slit2 expression in the tumor samples, with Log-rank test p-value displayed. **(E)** The Oncoprint graph summarizes genetic alterations in Slit2, Slit3 or Robo1 genes across 178 lung cancer samples from Cancer cBioPortal dataset. The row represents individual genes and each small column represents a tumor sample. The blue bar indicates homozygous deletion; the green squares represent point mutations and mRNA downregulation is depicted by light blue boxes. **(F)** Selected mutations of Slit2, Slit3 or Robo1 among lung cancer patients in TCGA dataset were shown above the diagram in the corresponding domains. **(G)** The plots demonstrated the relationship between expression of Slit2, Slit3 or Robo1 and CNA (DNA copy-number alterations) in lung tumors. Boxplots were divided by the putative CNA of genes (Homdel: homozygously deleted; Hetloss: heterozygously deleted; Diploid: two alleles present). mRNA levels of Slit2, Slit3 or Robo1 were measured by the number of RPKM (reads per kilobase per million reads sequenced) in the RNASeq data from lung carcinoma patients and expressed as Log2 median-centered intensity.

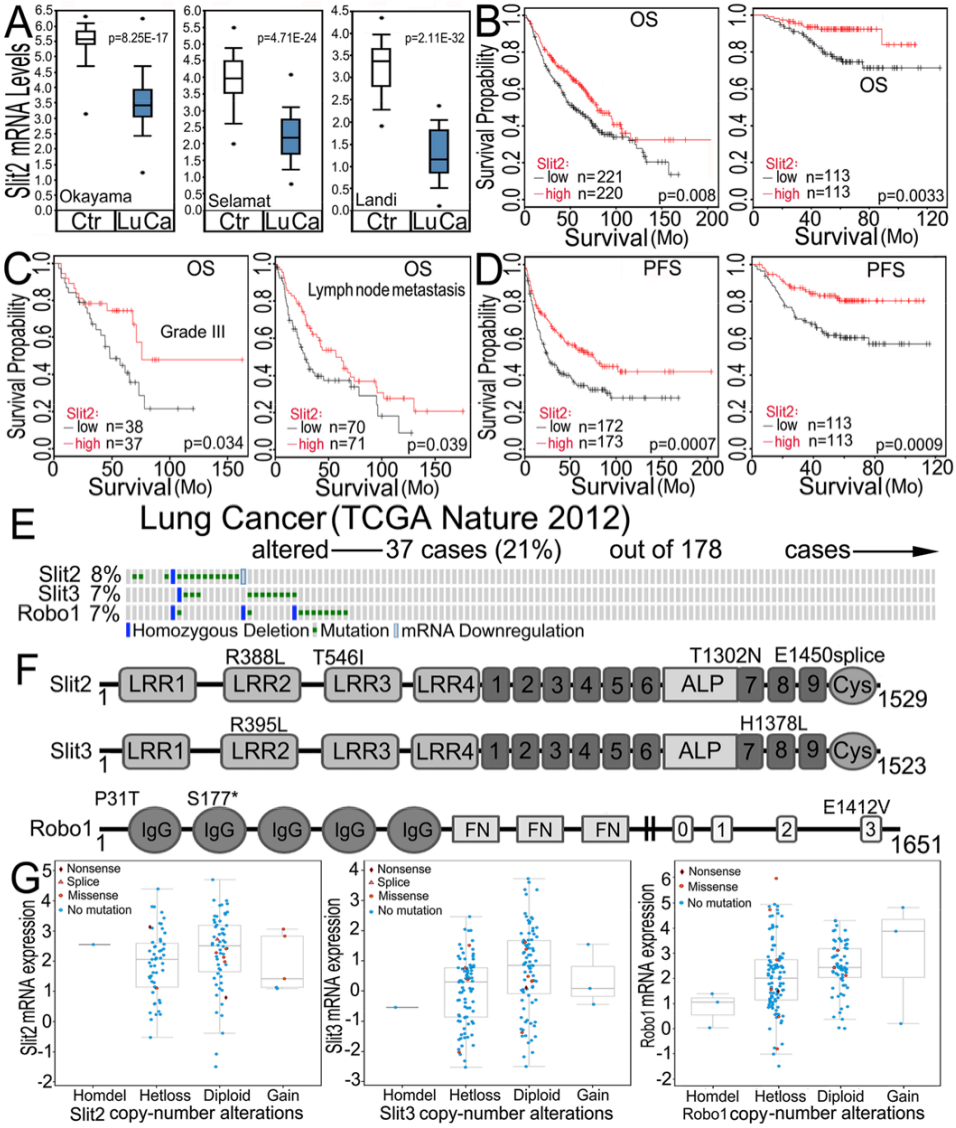

Supplemental Figure 10. The specificity of Myo9b antibody as demonstrated by immunohistochemical staining and western blotting. (A) Tissue sections from the subcutaneous H1299Ctr tumors in nude mice described in Figure 7 were stained with pre-immune IgG (Ctr), the purified Myo9b antibody preparation following antigen absorption (Abs) or the purified Myo9b antibody (Non-absorbed, Non-). The cytoplasmic yellow staining was only observed in the Myo9b antibody group, indicating that the Myo9b antibody specifically detected the endogenous Myo9b protein (Scale bar: 50um; n=10). **(B)** Myo9b immunostaining signals in panel A was quantified using ImageJ software. Data were presented as the mean ± SEM (three independent experiments; p value by Student's t test). **(C)** Purified Myo9b-GAP domain fused to glutathione S-transferase (GST) protein was used to prepare Myo9b antibody. **(D)** Western blotting assay using H1299 cell lysates prepared from control siRNA (siCtr) or specific siMyo9b treated cells. The Myo9b band signals detected by the purified Myo9b antibody were reduced by specific siMyo9b. **(E)** Quantification of Myo9b Western blotting signals in panel C, presented as the mean ± SEM (3 independent experiments; p value by Mann–Whitney test).

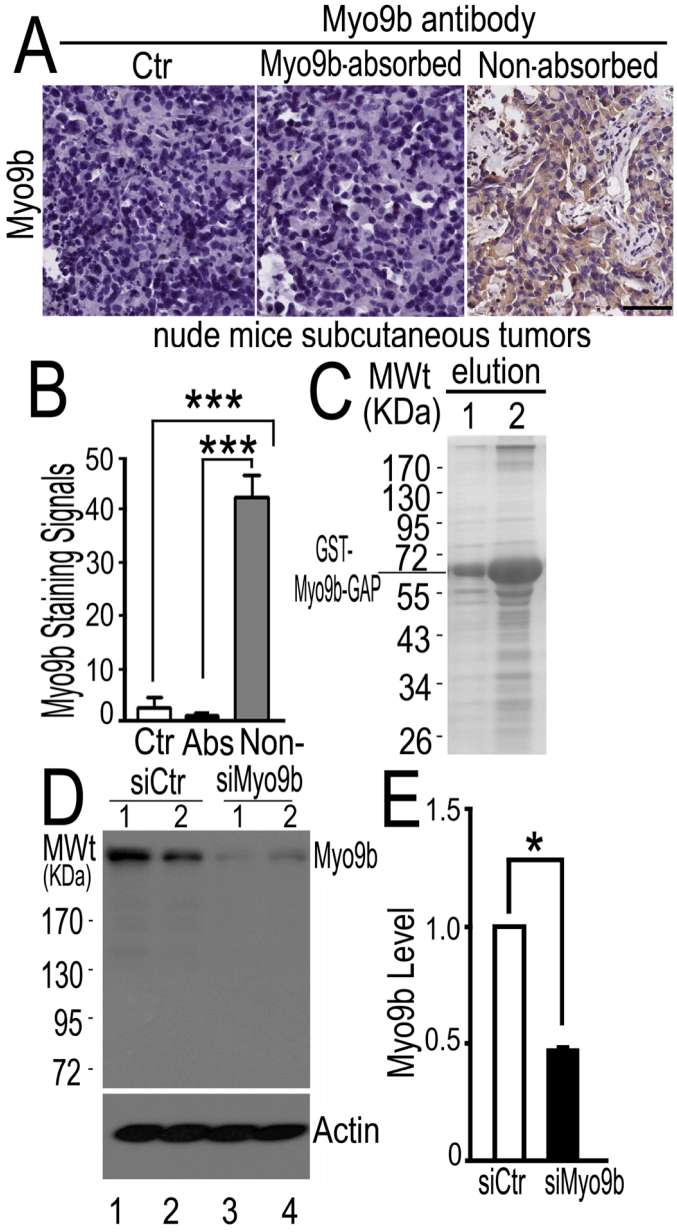

Supplemental Figure 11. Immunostaining of lung cancer samples using antibodies against Ecadherin, vimentin and Myo9b. Immunohistochemical staining was carried out using specific antibodies against E-cadherin, vimentin and Myo9b in the consecutive serial sections of a pathologically diagnosed human lung carcinoma sample. E-cadherin and vimentin proteins were utilized respectively as epithelial and mesenchymal markers respectively. Representative staining of these proteins in lung cancer is shown (Scale bars: 50um, 100um and 200um).

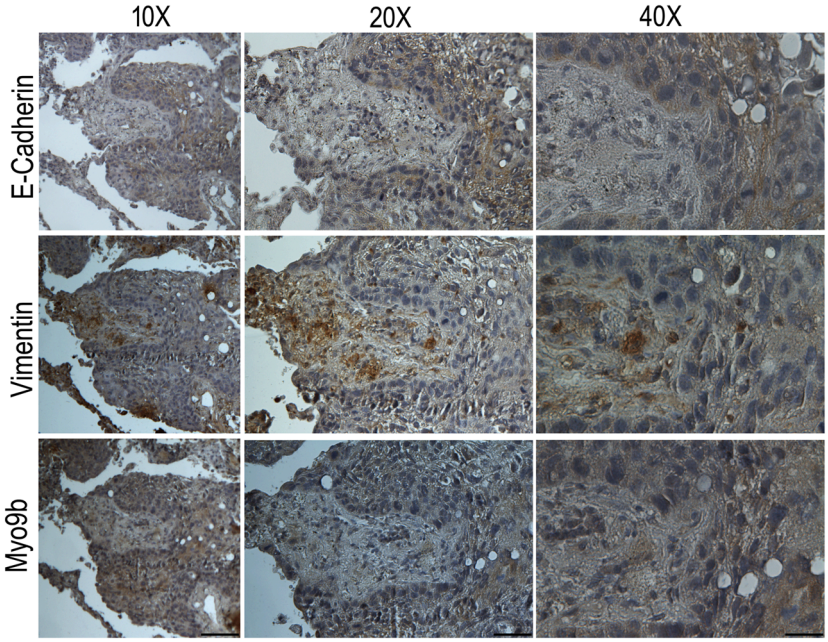

Supplemental Table 1. The number of mice with non-invasive tumors in the corresponding groups

Groups	Noninvasive Tumors with Smooth Borders	p (X^2 test)
Ctr	1/10	0.0345
Slit	5/7	

Supplemental Table 2. Fractions of mice with lung metastasis in two groups

Groups	Lung Metastasis	p (X^2 test)
Ctr	10/10	0.0031
Slit	3/10	

Supplemental Table 3. Correlation between Myo9b expression and clinicopathological features of lung cancer patients

Groups	Myo9b expression			p (X2 test)
	Low	High	n	
Age (years)				
< 60	8	18	26	0.7772
≥60	9	25	34	
Gender				
Male	13	32	45	1.0000
Female	4	11	15	
Tumor Size				
< 3cm	12	23	35	0.2599
≥3cm	5	20	25	
Lymph Node Metastasis				
N0	16	28	44	0.0251
N1+N2	1	15	16	
Tumor Stage				
I	10	8	18	0.0042
II-III	7	35	42	
Total	17	43	60	

Supplemental Methods

Cell culture

The lung cancer cell lines H1299, A549, H719, H841 and the human embryonic kidney cell lines HEK293 were from ATCC and cultured in Dulbecco's modified Eagle medium (DMEM) (Gibco) supplemented with 10% (v/v) fetal bovine serum (FBS) (Gibco), 100 u/ml of penicillin, and 100 ug/ml of streptomycin (P/S)(Gibco). HEK293 cells lines stably expressing either the vector control, Robo1-HA, Robo1N-HA or Slit2-Myc were described previously (4, 5). All cells were cultured in a 37°C, humidified, 5% CO_2-containing atmosphere incubator (Thermo Scientific).

Antibodies

Commercially available antibodies used in this study include anti-Flag (Sigma Aldrich/F3165), anti-Myc (Cwbiotech/CW0088), anti-HA (Cwbiotech/CW0092A), anti-GFP (Invitrogen/A6455), anti-His (Cwbiotech/CW0082), anti-RhoA (Santa Cruz Biotechnology/SC-418), anti-Cdc42 (BD Biosciences Pharmingen/610929), anti-Rac1 (BD Biosciences Pharmingen/610651), anti-Myo9b (ProteinTech Group, Inc/12432-1-AP), anti-Robo1 (ProteinTech Group, Inc/20219-1-AP), anti-Actin (ProteinTech Group, Inc/60008-1-Ig), anti-E-Cadherin (Abcam/ab76055) and anti-vimentin (Abcam/ab8978). The polyclonal anti-Myo9b antibody used in immunohistochemical analysis was raised in rabbits using purified Myo9b-RhoGAP domain fused to glutathione S-transferase protein and affinity-purified by Sino Biological Inc. The specificity of this polyclonal Myo9b antibody was demonstrated by immunohistochemical and Western blotting analyses (Supplemental Figure 10).

Plasmid constructs and Myo9b siRNAs

Plasmids expressing the full-length Robo1 and Robo1 deletion mutants tagged with a HA were described before (4, 33). Plasmids encoding myc-RhoA, myc-Cdc42, myc-Rac1 DN-RhoA or CA-RhoA were described previously (31). Human full-length Myo9b, which codes for the 2157-amino acid Myo9b protein, was generated by PCR amplification. For construction of the C1-GAP domain of Myo9b (1633-1983 aa), the fragment was amplified using the CMV-Sport6-Myo9b(EST: BC018108) (ProteinTech Group, Inc) as a template. The △GAP mutant (1-1411△1984-2157aa) was prepared with the template full-length Myo9b. All constructs were subcloned between the EcoR I (NEB) and Not I (NEB) sites of a 3×Flag-pCMV7.1 vector (Invitrogen). The plasmids containing mutations were constructed by overlap extension PCR. The RoboICD fragment was inserted into pET32a vector with an N-terminal MBP-His_6 tag using EcoR I and Sal I (NEB) sites. All constructs were verified by DNA sequencing. Two different siRNAs against Myo9b were synthesized together with a negative control siRNA (siCtr) (Shanghai Gene Pharma Co., Ltd). The sequences of siRNAs were as described in Supplemental Table 5. The siRNAs were transfected into H1299 cells using Lipofectamine 2000™ (Invitrogen) according to the manufacturer's instruction.

Immunoprecipitation and Western blotting

HEK293 or H1299 lung cancer cells were lysed in lysis buffer [20 mM HEPES-KOH (pH 7.4), 2 mM EDTA, 250 mM NaCl, 0.5% Nonidet P-40, 50mM NaF, 1mM PMSF, 1mM Na_3VO_4,10% glycerol and proteinase inhibitors (Roche)]. Insoluble materials were pelleted and supernatants were incubated with antibodies for 1 hr at 4°C, following further incubation with 30ul of a 50% suspension of protein A/G agarose beads (Roche) for another 3 hr at 4°C. 10% of total volume was used as "input". After beads were washed three times with lysis buffer, immunoprecipitated proteins were separated on SDS-PAGE and transferred onto PVDF membranes. The membrane was blocked with 5% nonfat milk and probed using specific primary antibodies, following incubation with HRP-conjugated secondary antibodies (Amersham). The bands were detected with the ECL system (Millipore) before exposure to X-ray films.

GST pull-down assay

GST-RBD or GST-PBD fusion protein was purified from E. coli and cleared with glutathione sepharose beads (Pharmacia) at 4°C for 2 hr. H1299 cells were washed twice with ice-cold PBS and lysed in cell lysis buffer [50 mM Tris-HCl (pH 7.4), 150 mM NaCl, 2mM $MgCl_2$, 1 mM DTT, 1% Nonidet P-40, 10% glycerol, proteinase inhibitors (Roche)]. Cell extracts were incubated with GST-RBD or GST-PBD immobilized to beads at 4°C for 2 hr. After washing three times, beads were boiled for 5 min and resolved on 15% SDS-PAGE. The Rho GTPases were determined by Western blotting probed with corresponding specific antibodies.

Wound-healing assay for cell migration

H1299 cells were seeded on glass coverslips containing photo-etched grids following coating with collagen. After cells became confluent, a wound area was created using a sterile 10ul pipette tip; and cells were allowed to grow after extensive rinses to remove floating cells. Ten images were taken at 0 hr and 12 hr following culture in the presence of the control or Slit-containing media. Cell migration was quantified by measuring the forward migration distance of cells from the line of wound formation.

Protein expression and purification

The cDNA encoding the RhoGAP domain of the human Myo9b protein (residues 1691-1916) was cloned into a modified pET32a vector that contains an N-terminal Trx-His_6 tag. The recombinant Myo9b RhoGAP protein was expressed in Escherichia coli (BL21-CodonPlus) cells at 16°C. The Trx-His_6-tagged fusion protein was purified by Ni2+-Sepharose 6 Fast Flow (GE Healthcare) affinity chromatography followed by size-exclusion chromatography (Superdex-200 26/60, GE Healthcare). After removal of the Trx-tag, the Myo9b RhoGAP domain was further purified by another round of size-exclusion chromatography.

RT-PCR and Real Time-PCR

Total RNAs from H1299, A549, H719, H841 and HEK293 cells were isolated using Trizol reagent (Invitrogen). cDNA synthesis was carried out using reverse transcriptase with an oligo (dT)18 primer (Invitrogen). Sequences of primers in polymerase reaction chain were shown in table S1. The PCR was carried out using following conditions: 3 min at 95°C for one cycle followed by 35 cycles of 1 min at 94°C, 1 min at 56°C (according to Tm) and 1 min at 72°C. RT-PCR products detected by agarose gel electrophoresis and followed by ethidium bromide staining.

Twenty five pairs of de-identified lung cancer and adjacent non-tumor tissue samples were obtained from consented patients in Tangdu Hospital, Xi'an, P. R. China with approved protocols and following Institutional and National Guidelines. Total RNA was isolated from the samples with Trizol reagents (Invitrogen). DNA was removed by treatment with RNase-free DNase (NEB). cDNAs were prepared with reverse transcriptase (Invitrogen). Real-time PCR was carried out using corresponding specific primers. Relative quantitation was determined using the ABI PRISM 7300 sequence detection system (Applied Biosystems) that measures real-time SYBR green fluorescence (Thermo Fisher Scientific, Waltham, MA) and then calculated by means of the comparative Ct method ($2^{-\Delta\Delta Ct}$) with the expression of GAPDH as an internal control. The primers used were as described in Supplemental Table 5.

Supplemental Table 4. Data collection and refinement statistics of Myo9b RhoGAP domain

Data collection	
Space group	$P2_12_12_1$
Unit cell parameters(Å)	a=77.1, b=85.0, c=134.1
Resolution range(Å)	50.0 - 2.20 (2.32 – 2.20)[a]
No.of unique reflections	45424(6528)
Redundancy	6.9(7.1)
I/σ(I)	10.5(3.0)
CC(1/2)	0.996(0.896)
Rpim	0.047(0.247)
Rmerge (%)[b]	11.3(61.5)
Completeness (%)	99.9(100.0)
Structure refinement	
Resolution (Å)	50.0 - 2.20 (2.25-2.20)
Rwork[c] / Rfree (%)[d]	20.7(25.5)/23.7(32.6)
R.M.S.D bonds (Å)/angles (º)	0.003/0.70
Average B factor	55.40
No. of atoms	
Protein atoms	6503
Water molecules	338
No. of reflections	
Working set	43349
Test set	1995
Ramachandran plot	
Most favored regions (%)	92.1
Additionally allowed (%)	6.4
Generously allowed (%)	0.8
Disallowed (%)	0.7

[a]The values in parentheses refer to the highest resolution shell.

[b]$R_{merge}=\sum_h\sum_i|I_i(h) - \langle I(h)\rangle|/\sum_h\sum_i I_i(h)$, where I is the observed intensity and $\langle I\rangle$ is the average intensity of multiple observations of symmetry-related reflection h.

[c]R_{work} is the R_{factor} for the working dataset. $R_{factor}=\sum||Fo|-|Fc||/\sum|Fo|$ where $|Fo|$ and $|Fc|$ are observed and calculated structure factor amplitudes respectively.

[d]R_{free} is the cross-validation R_{factor} computed for a randomly chosen subset of 5% of the total number of reflections, which were not used during refinement.

Supplemental Table 5. The primer pairs used in this study

RT-PCR primers		
Slit2	Forward primer:	5'-GGTGTCCTCTGTGATGAAGAG-3'
	Reverse primer:	5'-GTGTTTAGGAGACACACCTCG-3'
Robo1	Forward primer:	5'-GCATCGCTGGAAGTAGCCATAC-3'
	Reverse primer:	5'-GTGTATGAACCCATGTCACCAGC-3'
Myo9b	Forward primer:	5'-ATGAGTGT GAAAGAGGCAG-3'
	Reverse primer:	5'-CCACCAGCTGCATATGCA-3';
Actin	Forward primer:	5'-TCCCCCAACTTGAGATGTATGAAG-3'
	Reverse primer:	5'-AACTGGTCTCAAGTCAGTGTACAGG-3'
Real time PCR primers		
Slit2	Forward primer:	5'-GCATCCTAACTCCAAAGGGA-3'
	Reverse primer:	5'-CTTGTTGTCTTGGCAGTCGT-3'
Myo9b	Forward primer:	5'-CGAGAAGTTCAGGAGCAACA-3'
	Reverse primer:	5'-GACCAGGTTGGTGTCCTTCT-3'
GAPDH	Forward primer:	5'-GGAGCGAGATCCCTCCAAAAT-3'
	Reverse primer:	5'-GGCTGTTGTCATACTTCTCATGG-3'
Myo9b deletion mutants primers		
Myo9b-FL	Forward primer:	5'-AGTGAATTCATGAGTGTGAAAGAGGCAG-3'
	Reverse primer:	5'-AGTGCGGCCGCTCAGCCATTGGTCTGGC-3'
Myo9b-C1-GAP	Forward primer-1:	5'-AGTGCGGCCGCGCACGTGTTCGCCAGCTACCAGG TTAGCATCCCGCAGTCGTGCGAGCA-3',
	Forward primer-2:	5'-GCAGTCGTGCGAGCAGTGCCTCTCCTATATCTGGC TCATGGACAAGGCCCTGCTCTGCAGCGTGTG-3'
	Reverse primer:	5'-AGTGAATTCTTACCGGTAGGTGATGTCC-3'
Myo9b-△GAP	Forward primer:	5'-AGTGAATTCATGAGTGTGAAAGAGGCAG-3'
	Reverse primer:	5'-ATGTCTAGACCCGTTGTGCTCCTGGACA-3'
	Forward primer:	5'-ATGGTCGACCTGCCGGAGCTGGACCCAA-3'
	Reverse primer:	5'-AGTGCGGCCGCTCAGCCATTGGTCTGGC-3'
GAP point mutants primers		
GAP Wt	Forward primer:	5'-CCGGAATTCCCAGGCGTTGAGCCTGGCC-3'
	Reverse primer:	5'-ATAAGAATGCGGCCGCTCAAGCATTTTGTCGCAGGAG
GAP A1739E	Forward primer:	5'-CCGCAAGTCGGGTGAGGCCAACCGCACTCG-3'
	Reverse primer:	5'-CGAGTGCGGTTGGCCTCACCCGACTTGCGG-3'
GAP A1739N	Forward primer:	5'-CTCTACCGCAAGTCGGGTAATGCCAACCGCACT-3
	Reverse primer:	5'-AGTGCGGTTGGCATTACCCGACTTGCGGTAGAG-3
GAP A1739V	Forward primer:	5'-CGCAAGTCGGGTGTTGCCAACCGCACT-3'
	Reverse primer:	5'-AGTGCGGTTGGCAACACCCGACTTGCG-3'
GAP N1741E	Forward primer:	5'-GTCGGGTGCTGCCGAGCGCACTCGGGAGC-3'
	Reverse primer:	5'-GCTCCCGAGTGCGCTCGGCAGCACCCGAC-3'
GAP R1742E	Forward primer:	5'-CGGGTGCTGCCAACGAGACTCGGGAGCTCCG-3'
	Reverse primer:	5'-CGGAGCTCCCGAGTCTCGTTGGCAGCACCCG-3'
Cdc42 point mutants primers		
Cdc42S88D/K94P	Forward primer1:	5'-CCATCTTCATTTGAAAACGTGC CAGAAAAGTGGGTGCCTGAGAT-3'
	Reverse primer1:	5'-ATCTCAGGCACCCACTTTTCTG GCACGTTTTCAAATGAAGATGG-3'

	Forward primer2:	5'-CTGTTTTTCAGTGGTCTCTCCAG ATTCATTTGAAAACGTGCCAGAA-3'
	Reverse primer2:	5'-TTCTGGCACGTTTTCAAATGAAT CTGGAGAGACCACTGAAAAACAG-3'
Rac1 point mutants primers		
Rac1A88D/R94P/A95E	Forward primer1:	5'-GCATCATTTGAAAATGTCCCT GAAAAGTGGTATCCTGAGGTG-3'
	Reverse primer1:	5'-CACCTCAGGATACCACTTTTC AGGGACATTTTCAAATGATGC-3'
	Forward primer2:	5'-GCTTTTCCCTTGTGAGTCCTGA TTCATTTGAAAATGTCCCTGAA-3'
	Reverse primer2:	5'-TTCAGGGACATTTTCAAATGAA TCAGGACTCACAAGGGAAAAGC-3'
Myo9b siRNAs		
siMyo9b-1	Forward primer:	5'-CGAGAUCACGAUGCACUGGTT-3'
siMyo9b-2	Forward primer:	5'-AGCUGUUCCUCUCGAAGUCTT-3'
siCtr	Forward primer:	5'-UUCUCCGAACGUGUCACGUTT-3'